Title

Fault controlled geometries by inherited tectonic texture at the southern end of the East African Rift System in the Makgadikgadi Basin, northeastern Botswana

Authors

Schmidt, G
Franchi, F
Salvini, F
et al.

Publication Date

2023

DOI

10.1016/j.tecto.2022.229678

Peer reviewed

Tectonophysics 846 (2023) 229678

Contents lists available at ScienceDirect

Tectonophysics

journal homepage: www.elsevier.com/locate/tecto

Fault controlled geometries by inherited tectonic texture at the southern end of the East African Rift System in the Makgadikgadi Basin, northeastern Botswana

G. Schmidt [a,*], F. Franchi [b], F. Salvini [a], A.T. Selepeng [b], E. Luzzi [c,f], C. Schmidt [d], E.A. Atekwana [e]

[a] Department of Science, Università degli studi Roma Tre, Rome, Italy
[b] Department of Earth and Environmental Science, Botswana International University of Science and Technology, Palapye, Botswana
[c] Department of Physics and Earth Sciences, Jacobs University Bremen, Bremen, Germany
[d] Department of Geological and Environmental Sciences, Western Michigan University, Kalamazoo, MI, United States of America
[e] Department of Earth and Planetary Sciences, University of California, Davis, CA, United States of America
[f] Bay Area Environmental Research Institute, Moffett Field, CA, United States of America

ARTICLE INFO

Keywords:
Botswana
Makgadikgadi basin
Paleolake
Fault geometry
Tectonic terrane

ABSTRACT

One of the three narrow rift belts that mark the southern end of the East African Rift System (EARS) intersects the Makgadikgadi Basin of northeastern Botswana. Although tectonic activity in the region is known to have influenced the evolution of these pans, the interrelationship between shoreline geometry, fault strikes, and the intersection of the underlying tectonic terranes has yet to be fully realized. We analyzed faults and subsurface structures in the region of the pans using a field investigation in combination with satellite imagery and geophysical data, to constrain the influence that the regional tectonic regime has had on the formation of the present-day pan geometry. We find that pan shorelines are controlled by the intersection of three preferred fault orientations which can be understood in the context of the "older" terranes they overlie, namely the Magondi Belt and the Limpopo Belt. We propose that the pronounced curvature of the southern Magondi Belt has influenced the eastward curvature of the rift-related faults and was likely produced by the impingement of the developing fold belt on the Zimbabwe Craton. Furthermore, limited focal mechanism solutions data from earthquakes north and south of the pans suggests a change in regional extension direction from NW-SE to NE-SW. Determining the relationship between these fault orientations and the underlying tectonic terrains is an important step in understanding the formation of the Makgadikgadi Basin, and more broadly the current tectonic regime of Botswana. The evidence of fault-controlled shorelines within an evaporitic environment may also have implications for regional groundwater activity.

1. Introduction

The southwestern branch of the East African Rift System (EARS) trends toward the southwest from the Tanganyika and Rukwa Rifts in Tanzania, through the Luangwa Rift Zone and Kafue rifts in Zambia, and into northern Botswana where it is characterized by a diffuse zone of rifting (Fig. 1) (Modisi et al., 2000). In northern Botswana the EARS is composed of two Quaternary rift zones which are separated by the Neoproterozoic-early Paleozoic aged Passarge Basin (Daly et al., 2020; Fadel et al., 2018; Key and Ayres, 2000; Modisi et al., 2000; Singletary et al., 2003) (Fig. 1b): 1. The Okavango Rift Zone (ORZ) is approximately 150 km wide and characterized by a northeast-southwest-trending set of normal faults that terminate against, a west-northwest-trending dextral shear zone called the Sekaka Shear Zone (Modisi et al., 2000; Kinabo et al., 2007, 2008; Bufford et al., 2012). 2. The normal faults that compose the more easterly of the two zones, herein called the Lake Kariba Rift Zone (LKRZ), which trend southwesterly from Lake Kariba into northeast Botswana where they bend sharply eastward in a region known as the Makgadikgadi Basin (Fig. 1b).

This study focuses on the structural history of the Makgadikgadi Basin, once occupied by the paleo-Lake Makgadikgadi (Burrough, 2022; Baillieul, 1979; Franchi et al., 2020, 2022; Grey and Cooke, 1977; McFarlane and Eckardt, 2006; Podgorski et al., 2013). This system developed in the Early Pleistocene (Moore et al., 2012) within the ca.

* Corresponding author.
E-mail address: genewalter.schmidt@uniroma3.it (G. Schmidt).

https://doi.org/10.1016/j.tecto.2022.229678
Received 20 June 2022; Received in revised form 21 November 2022; Accepted 25 November 2022
Available online 9 December 2022

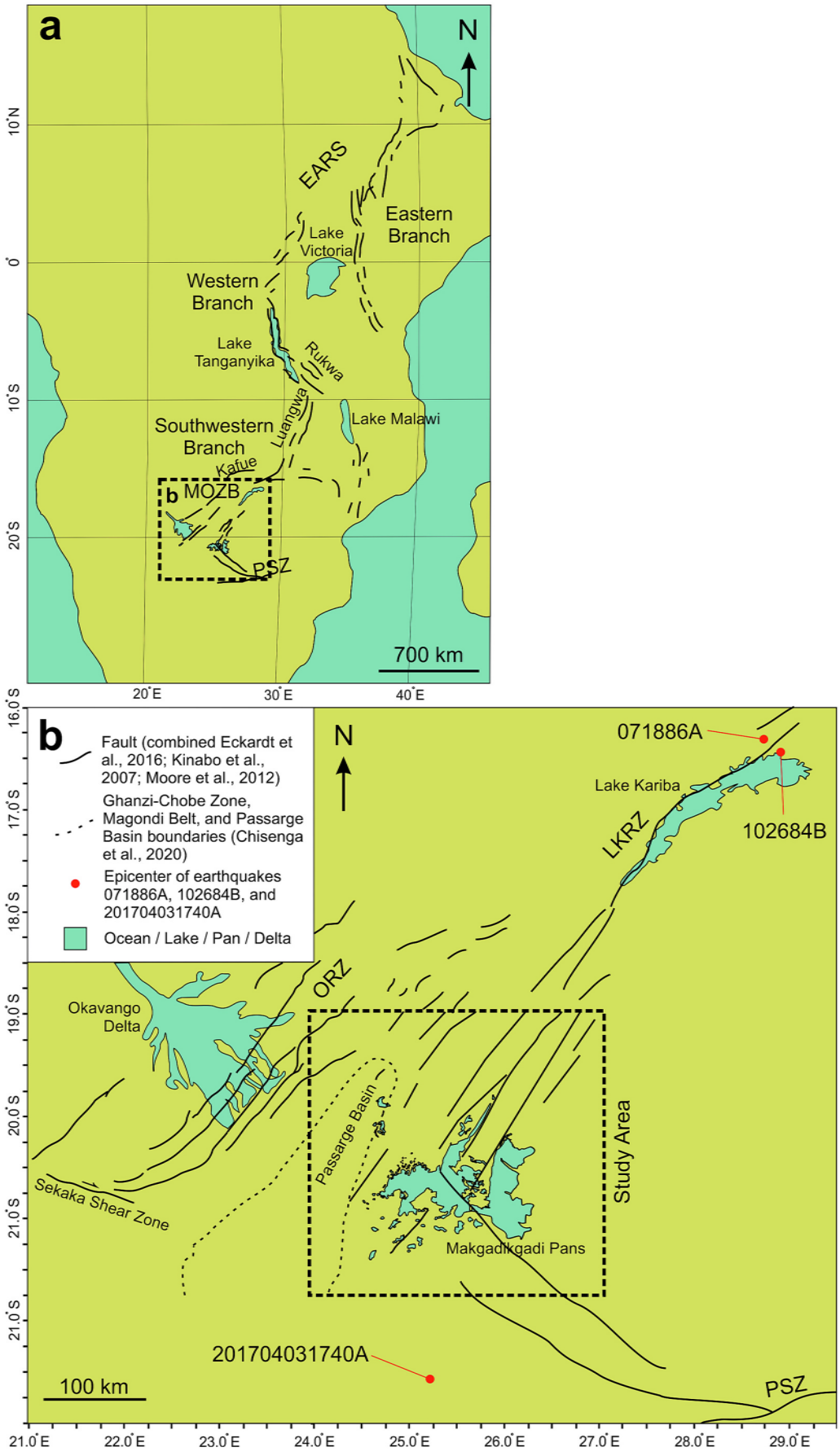

Fig. 1. a) Simplified map (Mercator projection) of specific elements of the East African Rift System (EARS) (modified from Kinabo et al., 2007 and Evans et al., 2019). Bold lines mark scarps and faulting associated with various branches of the EARS. PSZ: Palala Shear Zone. b) The Makgadikgadi-Okavango-Zembezi basin (MOZB) contains the southwestern most branch of the EARS comprised of the Okavango Rift Zone (ORZ) and the Lake Kariba Rift Zone (LKRZ), which intersects with the Makgadikadi Pans. Numbers on the three earthquake epicenters are from the Global Centroid-Moment-Tensor (CMT) catalog (Dziewonski et al., 1981; Ekström et al., 2012). Dashed box indicates the location of the study area outlined in Figs. 2 and 5–10.

120,000 km^2 Makgadikgadi-Okavango-Zambezi Basin (MOZB) as part of the southwestern branch of the EARS (Riedel et al., 2014; Schmidt et al., 2017) (Fig. 1a). Its evolution is controlled by northeast-southwesterly striking faults closely related to EARS propagation toward the southwest (Modisi et al., 2000; Kinabo et al., 2007). The Makgadikadi Pans are the salt-flat remnants of a 90,000 km^2 lake which was present about 2 mya and disappeared by evaporation when fault movements diverted the river that fed the lake (Franchi et al., 2022; Riedel et al., 2014). The specific pans include the Ntwetwe (surface area > 3400 km^2), the Sua (surface area > 2800 km^2), and several other smaller pans (Fig. 2a). The pans are relatively flat (903–905 m) with "shorelines" that are 5–10 m higher. The stratigraphy of the pans includes a 30–150 m thick cover of fluvio-lacustrine mudstones and sandstones of the Cretaceous-Neogene Kalahari Group (Franchi et al., 2020; Ringrose et al., 2009; Thomas and Shaw, 1991). These formations are underlain by Early Permian mudstones and sandstones of the Ecca Group (Green et al., 1980; Ringrose et al., 2009). The Early Jurassic (180 Ma) Okavango Dike Swarm runs NW-SE through the study area (Baillieul, 1979; Le Pera, 2014). The pans region also overlies the intersection of three tectonic terranes: the Mesoproterozoic NE-SW trending Magondi Belt, the older Archean-Paleoproterozoic NW-SE trending Limpopo Belt, and the Archean Zimbabwe Craton (Majaule et al., 2001) (Fig. 3).

The close relationship between geometry and regional structural features provides an opportunity to understand the way in which the EARS propagated to the southwest. Consequently, the Makgadikadi Pans represent an opportunity to not only constrain pan formation, but understand the ongoing tectonic progression of the EARS. The goal of this study is to examine the geometry and kinematics of the faults within the pans and surrounding area and evaluate the relative influence of these older tectonic terranes on the location, orientations, and movements of faults in this branch of the EARS. These analyses contribute to our comprehension of African Quaternary geology and provide a framework for interpreting the surficial features and buried structures of the Makgadikadi Basin. Additionally, investigations of faulting in the pans may also advance our understanding of the movement of groundwater in northeastern Botswana.

2. Geological setting and previous work

2.1. Faults and topographical features

Faults within the perimeter of the Makgadikgadi Pans, as identified by their surface expressions, were first identified by Baillieul (1979), and updated by various works including Barton Jr et al. (1994), Key and Ayres (2000), Moore et al. (2012), and Eckardt et al. (2016). The faults strike northeast-southwest and are interpreted to be a system of graben and half-graben extending from the LKRZ (interpreted from Baillieul, 1979; Eckardt et al., 2016). Baillieul (1979) first proposed these faults extending from the northeast had affected the shape of the present-day pans. Seismic data indicates that many of these faults are deep and not simply surface features (e.g. Baillieul, 1979), however their exact age is poorly constrained.

The N-S trending Gidikwe Ridge (Fig. 4b) represents an ancient shoreline during a period of the Neogene history of the pans (McFarlane and Eckardt, 2006; Podgorski et al., 2013) and is an important geomorphological features of the basin. It is an arcuate fossil sand ridge that stretches for >200 km along the western margin of the Makgadikgadi Basin (Grove, 1969; Grey and Cooke, 1977; Cooke, 1980; Burrough et al., 2009). The ridge has a crest elevation close to 945 m (Grey and Cooke, 1977; Cooke, 1980). The sand from the base of the Gidikwe ridge has a mean grain size composition of ca. 0.125 mm (0.2 mm according to more recent studies from Burrough et al., 2009), it is rich in calcite and contains abundant shell material, i.e. ostracodes, indicating a lacustrine origin for these sediments (Cooke, 1980).

Faults within the Limpopo-Shashe Belt tectonic terrane east and southeast of the pans have been mapped previously extending northwest from the Palala Shear Zone (PSZ) (Mapeo et al., 2004; Ranganai et al., 2002; Schaller et al., 1999) (Fig. 1). One of these faults, the Lechana

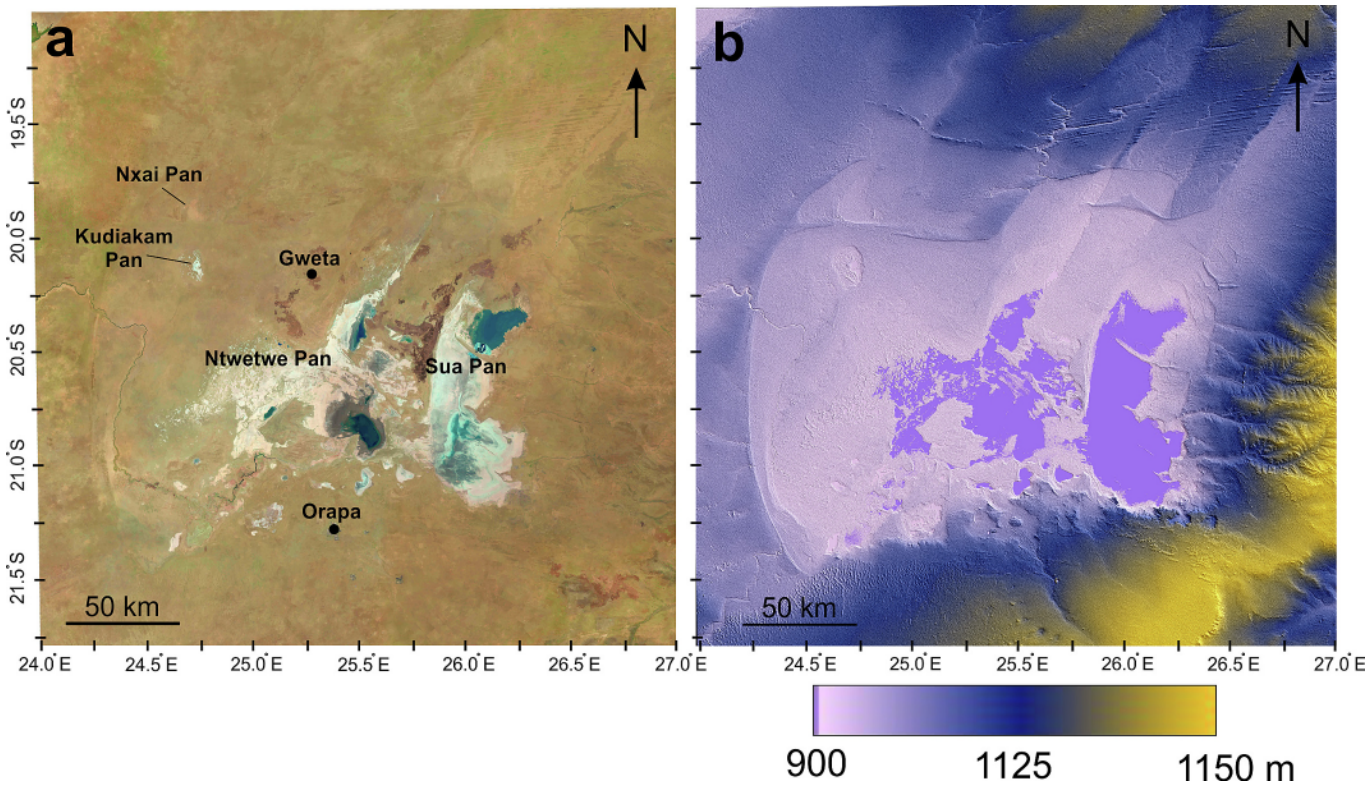

Fig. 2. Study location. a) Landsat 8 satellite mosaic from October 2021 b) Hillshaded Digital Elevation Model (DEM) showing the topography of the study area. UTM projection.

Fault enters the area of the pans reaching as far as Gweta (Aldiss and Carney, 1992; Carney et al., 1994) (Figs. 1, 3a, and 4b). Where the Lechana Fault was mapped in the Paleoproterozoic bedrock outside of the area of the pans, it and other NW-striking faults were interpreted to be strike slip (e.g., Mapeo et al., 2004). Aldiss and Carney (1992) show it to have left separation. However, it is unlikely that the movement on this fault as shown in Paleoproterozoic rocks has the same movement direction in the Quaternary sedimentary strata of the pans.

Another fault identified in the bedrock terrane east of Sua Pan is the Bushman Fault (Fig. 4b) and associated Bushman Shear Zone (approximately 300 m wide) (Barton Jr et al., 1994; Kooganne et al., 2021) which strikes N-S and hosts a variety of ore deposits dominated by hydrothermal alteration mineral assemblages (Kooganne et al., 2021).

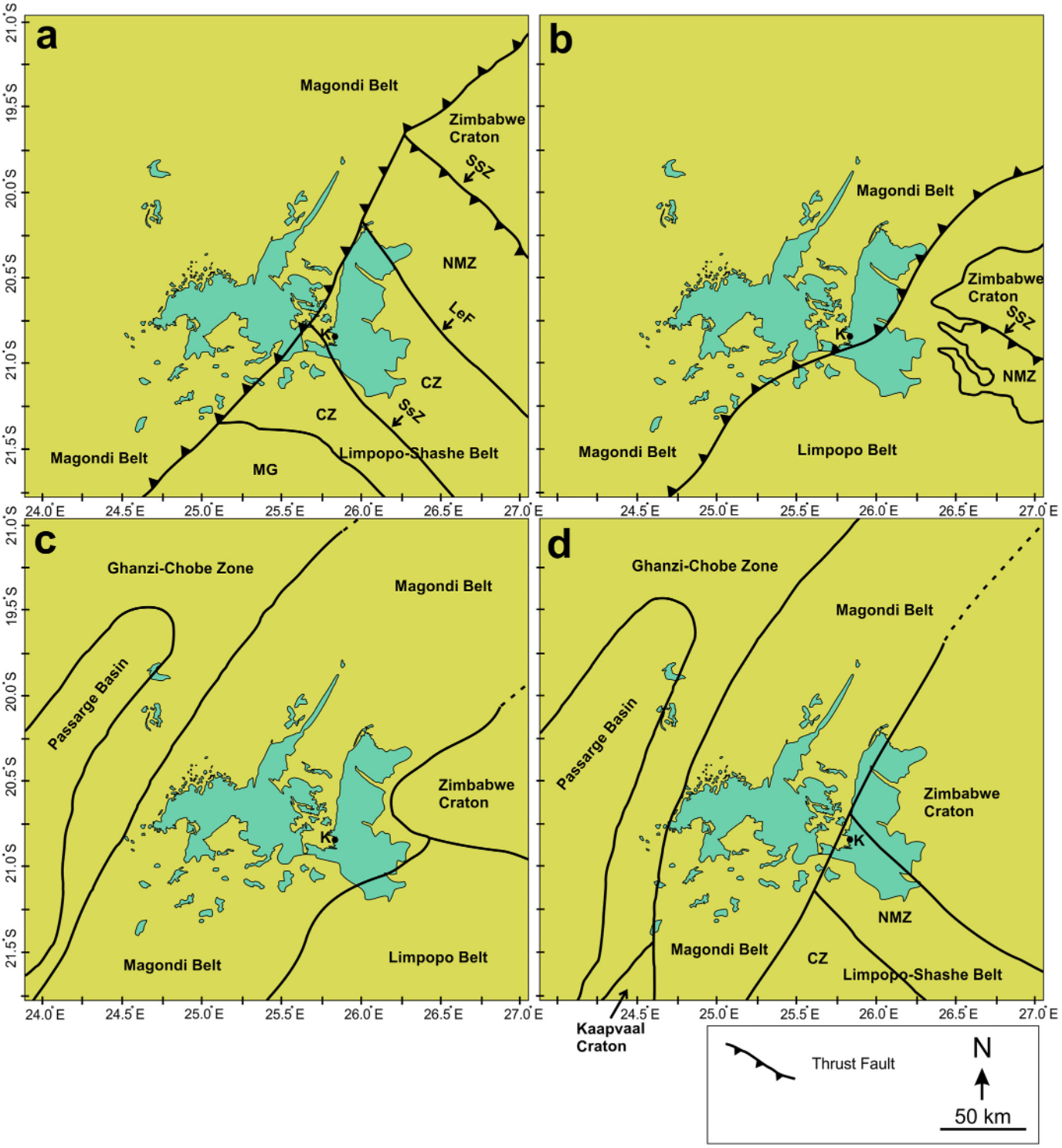

Fig. 3. Combined interpretations of the tectonic terrane boundaries within the study area. a) from Ranganai et al. (2002) b) McCourt et al. (2004). c) Singletary et al. (2003). d) Chisenga et al. (2020). K = Kubu Island, NMZ = Northern Marginal Zone, CZ = Central Zone, MG = Mahalapye Granite Complex, SSZ = Shashe Shear Zone, SsZ = Sunny Side Shear Zone, LeF = Lechana Fault.

2.2. Underlying tectonic terranes

Five tectonic terranes have been previously proposed to be present within the study area (Chisenga et al., 2020; McCourt et al., 2004; Ranganai et al., 2002; Singletary et al., 2003) (Fig. 3). These terranes, in order of decreasing age are: the Zimbabwe Craton (Archean), the Limpopo-Shashe Belt (Archean-Paleoproterozoic), the Magondi Belt (Paleo-Mesoproterozoic), the Passarge Basin (Neoproterozoic), and the Ghanzi-Chobe Zone (Neoproterozoic). A small section of the Kaapvaal Craton was proposed to be present in the study area by Chisenga et al. (2020) (Fig. 3d), but is absent in the other studies. The Shashe Belt is technically a separate fold belt in contact with the Zimbabwe Craton and is surrounded by the Limpopo Belt. For the purposes of this study, we refer to the Limpopo and Shashe Belts simply as the Limpopo-Shashe Belt, as does Ranganai et al. (2002) and Chisenga et al. (2020). However, in many studies the area is often simply referred to as the Limpopo Belt.

The Zimbabwe Craton, the Limpopo-Shashe Belt, and the Magondi Belt have been previously proposed to intersect within the location of the pans (Fig. 3). McCourt et al. (2004) and Ranganai et al. (2002) proposed that the Magondi is thrust over the Zimbabwe Craton and Limpopo-Shashe Belt. Ranganai et al. (2002) also proposed that the boundary between the Limpopo-Shashe Belt and the Zimbabwe Craton was bounded by the Shashe Shear Zone. Unfortunately these works did not include reference to the Makgadikgadi Pans location which can now be fully appreciated (Fig. 3). By appreciating the differences between these four previous interpretations, and visualizing their direct relationship to the pans, the location of the tectonic terrane boundaries can be understood better. Furthermore, the influence that the tectonic terranes might have had on the pan geometry can be proposed.

The Zimbabwe Craton is an Archean (2.6–2.7 Ga) granitoid greenstone terrain containing five distinct "complexes" (McCourt et al., 2004). Rather than being an isotropic mass, the craton is a complex of different lithologies and fabrics. It is located northeast of the Sua Pan. However, for approximately 25 km east of the pan, the exact position of its boundary with the younger Limpopo Belt to the south is poorly constrained due to Quaternary cover. There have been several interpretations of the location of this boundary beneath the cover (Fig. 3). Where exposed, the craton contains foliation fabrics that trend in an eastward-concave arc (from northeast trending to northwest-trending) (McCourt et al., 2004, Fig. 3b) and shift to a uniform northwest-southeast trend, following a major northeast-verging shear zone (Shashe Shear Zone) (McCourt et al., 2004). The position of the western margin of the craton is also poorly constrained and has previously been proposed to extend below the Sua Pan (Chisenga et al., 2020), east of the Sua Pan (McCourt et al., 2004), or just northeast of the Sua Pan (Ranganai et al., 2002) (Fig. 3).

The Archean-Paleoproterozoic Limpopo-Shashe Belt tectonic terrane is interpreted to be a suture zone resulting from a collision between the Zimbabwe Craton and the Kaapvaal Craton to the south (Ranganai et al., 2002). It wraps around the southern part of the Zimbabwe Craton in a concave-northward arc (Chisenga et al., 2020; Majaule et al., 2001; McCourt et al., 2004; Miensopust et al., 2011; Ranganai et al., 2002; Singletary et al., 2003). At approximately 30.0° E, near the Zimbabwe-Botswana border, it changes trend from northeast -southwest (Limpopo Belt) to northwest-southeast (Shashe Belt). From the perspective of its possible influence on Cenozoic faulting in the area of the Makadikigadi Pans, the structure of the Shashe Belt is the pertinent part of this terrane. Ranganai et al. (2002) divided this approximately 250 km-wide belt into three subparallel, northwest-trending shear zones, the Northern Marginal Zone (NMZ), Central Zone (CZ) and Southern Marginal Zone (SMZ) (Fig. 3a and b). A more recent re-interpretation of the gravity and magnetic data (Chisenga et al., 2020) also refers to this part of the Shashe Belt at the contact with the craton as the Shashe Shear Zone, however placing the contact further south than the gravity anomaly used by Ranganai et al. (2002) as a marker for the contact.

The northeast-striking normal faults and their curved fault traces in the area of the pans lie within the Magondi Belt, the Passarge Basin, and the Ghanzi-Chobe Zone (Figs. 3 and 4b). The Magondi Belt is a Paleo-Mesoproterozoic orogenic/fold belt composed of a sequence of at least 5 km thick sequence of Paleoproterozoic metasedimentary and volcanic rocks (Magondi Supergroup) deposited along the western margin of the Zimbabwe Craton and later deformed in an east-to southeast-vergent fold thrust belt (Aldiss and Carney, 1992; Begg et al., 2009; Majaule et al., 2001; Hanson, 2003; Miensopust et al., 2011; Key and Ayres, 2000; Ranganai et al., 2002; Singletary et al., 2003). The northeast trend of this fold belt and pronounced eastward curvature of these earlier structures that occur below the overlying normal faults has been previously recognized (e.g. Majaule et al., 2001). The Ghanzi-Chobe Zone is a northeast trending linear belt of volcano-sedimentary rocks (Modie, 2000) and the Passarge Basin is a Neoproterozoic sedimentary basin within the Ghanzi-Chobe Zone (Chisenga et al., 2020; Modie, 2000) (Fig. 3c and d).

There is a $> 60{,}000\ m^2$ isolated outcrop of granite located on the western shoreline of the Sua Pan called Kubu Island (Fig. 3b) (Majaule et al., 2001). The granite is thought to be emplaced by intrusions through an Archean crust which occurred approximately 2.0 Ga (Majaule et al., 2001). Aldiss and Carney (1992) and Majaule et al. (2001) indicated Kubu Island is characterized by intense vertical jointing, however actual measurements of their orientations have not been conducted. The precise location of the boundary between the Magondi Belt (Proterozoic) and the Limpopo-Shashe Belt (Archean) is not known, however Kubu Island has been suspected to mark either the contact between the Magondi and Limpopo-Shashe Belts (McCourt et al., 2004) or a possible buried triple junction (Majaule et al., 2001). In as much as McCourt et al. (2004) and Ranganai et al. (2002) proposed that the Magondi Belt is thrust over the Limpopo-Shashe Belt, the presence of this isolated outcrop of granite at this location is poorly understood. Majaule et al. (2001) demonstrated that, although zircon dating from the granite shows that Kubu Island contains Archean aged crustal components, it actually lies within the Magondi Belt due to foliations which indicate that its placement occurred before the Magondi deformation period ended. Thus, Kubu Island is a valuable marker in that it locates the minimum southeastern extent of the Magondi Belt.

3. Methods

In addition to field investigation of the pans, carried out in October 2021, we used remote sensing techniques to constrain fault locations and orientations, as well as the underlying tectonic terrane boundaries and structure. Ten Landsat 8 images (with a resolution of 30 m/px) acquired in October 2021 (Fig. 2a) were used as the basis for regional context mapping (Fig. 4b). Elevation data from the Shuttle Radar Topography Mission (SRTM) forms our Digital Elevation Model (DEM; with a resolution of 28.7 m/px) which is presented in a "thermal" color ramp following Crameri et al. (2020) (Fig. 2b). We highlighted topographic trends observed in the DEM by implementing the "Least Squares Regression ->Nearest Neighbor Differences->Convolution Filtering" method written and described in Minin (2016). Pixels are then given a color based on dip direction. This process was integrated into a Python script to create Fig. 4a. The result of this process highlights the slope of all surface features so that the dip direction of linear features in the topography can be easily visualized. This aids the identification of fault scarps.

Faults were mapped by expanding upon known fault locations by tracing fault scarps that terminated at the edges of the pans and were traced across to where they matched with scarps on the adjacent side. A total of 28 faults were mapped and measured by use of the DEM filter (Fig. 4b). Fault azimuths were then plotted as rose diagrams using the Daisy software (Salvini et al., 1999). Moment tensor data from three earthquakes cataloged as 071886A, 102684B, and 201704031740A in The Global Centroid-Moment-Tensor (CMT) catalog (Dziewonski et al.,

1981; Ekström et al., 2012) were plotted into stereonets using the Daisy software (Salvini et al., 1999) and provided the relative movement of one group of NE-SW-striking faults and another group of NW-SE striking faults (Fig. 5).

Within the GIS environment Surfer® v22 (Golden Software, LLC), we processed aeromagnetic data to create a total magnetic intensity map to further assist in fault identification. The total magnetic intensity map allowed us to locate areas where NW-SE-trending dikes of the Okavango Dike Swarm are laterally offset. In addition, because the wider NNE-SSW trending magnetic highs are parallel to existing surficial fault scarps, we were able to discover faults that had no obvious surface expression. This allowed the identification of an additional eleven faults that were not verifiable from the DEM filter, making a total of 39 identified faults. Tectonic terrane boundaries were investigated with the assistance of a bouguer gravity anomaly map by tracing the outlines of major anomaly trends and referencing them to trends observed in the total magnetic intensity map and the DEM filter. All data were integrated into the GIS software Global Mapper v15.2 (Blue Marble Geographics, 2011).

4. Results

4.1. Fault identification and shoreline geometry

The identification of 28 fault scarps and their dip direction was achieved through tracing of features revealed in the color-coded filtered DEM (Fig. 4). Several of these scarps were observed to have an eastward curvature where they enter the pan area from the north, specifically at the Gidikwe Ridge and the northwestern corners of the Ntwetwe and Sua Pans (Fig. 4b). In the case of the Gidikwe Ridge and the western shoreline of the Sua Pan, a N*E*-SW striking fault dipping to the east curves to a N-S strike. The curvature of the Gidikwe Ridge is significant, with an approximately 80° change in strike (from 50° to 130°). Just east of the Gidikwe Ridge, a parallel fault scarp dips to the west and passes directly along the eastern shoreline of the Kudiakam Pan before it becomes the pathway for the Boteti River to the south (Fig. 4b). This gives the impression that the pans themselves have shorelines that are fault-controlled, most notably the western shoreline of Sua Pan (interpreted to be an eastward-dipping normal fault), the northeastern shoreline of Ntwetwe Pan (interpreted to be a northwestward-dipping normal fault), and the northwestern shoreline of Ntwetwe Pan that we interpret to be a southeastward-dipping normal fault (Fig. 4b).

The area of the pans also contains several NW-SE-striking faults, most notably the Lechana Fault that forms the southern boundary of Sua Pan (Fig. 4b). The Lechana Fault can be extrapolated to the northwest to where it right-separates the northeast-striking normal fault that borders the northeast side of the Ntwetwe Pan. It is important to emphasize that the apparent separation is not an unequivocal indication of strike slip. The Lechana Fault also appears to be truncated by the northeast-striking normal fault that defines the northwest border of the Ntwetwe Pan. To the southeast, the Lechana Fault curves northward across the southern boundary of Sua Pan and follows the general trend of the Lechana Fault as it was originally mapped in Paleoproterozoic basement rocks (Aldiss and Carney, 1992; Mapeo et al., 2004). The highlighted topographic data (Fig. 4a) indicates a northeast dip of the fault. Accordingly, we interpret the Lechana Fault here as a down-to-the-northeast normal fault. This is compatible with the NE-SW extension inferred from the focal mechanism of the 2017 Mw 6.5 Botswana earthquake to the south (Fig. 5). Actual slip direction is indeterminate.

Two other northwest-striking faults occur in the southwestern part of the Ntwetwe Pan. They strike in a slightly more westerly direction than the Lechana Fault described above. The southernmost of these faults left-separates the northwest-dipping normal fault that defines a portion of the southeastern boundary of the Ntwetwe Pan. The separation on the other of these two faults is not well-defined, but we have shown it with left separation because the two faults are parallel (Fig. 4b). As in the case of the Lechana Fault, the actual sense of fault slip is unknown. Both faults change strike to a more northerly direction and become curved to concave northeast, mimicking the curvature of southernmost part of the Gidikwe Ridge fault (Fig. 4b). Topographically these faults also dip northeast here (Fig. 4b), and we interpret them to be down-to-the-northeast normal faults, without knowing the actual slip direction.

There is an apparent ambiguity in the observation that the southern two of the northwest-trending faults that control parts of the eastern boundary of Ntwetwe Pan show left separation of the northeast-trending normal fault and the Lechana Fault to the north, with nearly the same NW strike, shows a right separation of the normal fault. One possible explanation of this"ambiguity" is that the extension direction changed over time, from NW-SE (left separation) to more E-W (right separation). A simpler explanation would be that the intersecting faults below the pans produced a step-like geometry that influenced the boundaries of the pans during sediment deposition, as the large parent lake was evaporated to the present pan geometry. The fact that the faults are discontinuous, because their traces are covered by sediment for long stretches, argues in favor of this explanation.

A set of five WNW-ESE-striking faults are located east of Sua Pan. Two of these faults curve northward where they enter the eastern border of Sua Pan and form high relief lineaments that are similar in shape to jetty or spit-like structures (Fig. 6). These two faults right separate a west-dipping normal fault which runs parallel to the Bushman Fault. The Bushman Fault is verifiable in the DEM (Fig. 6), can be faintly observed in satellite imagery and magnetic data, and has been identified previously from field mapping (Barton Jr et al., 1994). One of these faults appears to terminate against the fault parallel to the Bushman Fault (Figs. 4b and 6).

The northeast-southwest striking rift related faults enter the pans from the northeast, extending from the LKRZ (Fig. 1b). Although the LKRZ has less seismicity than the more northern rift zones in the EARS, two earthquakes (071886A and 102684B) that occurred immediately north of Lake Kariba (Fig. 1b) have fault plane solutions, presented previously by Kebede and Kulhánek (1991) and Hlatywayo (1995), that are useful in interpreting fault movements in the region of the Makgadikgadi Basin to the south (Fig. 5). The 1986 earthquake 0171886A (5.2 MW) has nodal planes that indicate a T-axis that is nearly horizontal and oriented approx. 140 (NW-SE extension). Either of the two nodal planes could be the actual fault, but the extension direction is clearly normal to the rift zone. For the 1984 earthquake 102684B (5.3 MW) the steeper of the two nodal planes is more likely the fault plane (strike 16, dip 77 SE). The T-axis plunge and trend is somewhat more northerly oriented than in the 1986 event, but it helps to establish an extension direction that is compatible with normal, dip-slip, faulting for the LKRZ.

Another, more recent earthquake (201704031740A), occurred approximately 200 km directly south of the southern limit of the pans (Fig. 1b). It occurred on a NE dipping normal fault within the southern Shashe Belt of the Limpopo Belt (Kolawole et al., 2017). The fault plane solution for the 6.5 Mw event has a nearly horizontal T-axis azimuth of 44^0 with an aftershock T axis of 26^0 (Fig. 5). The combined moment tensor data, though limited, was useful in determining the nature of the fault movements in the pans.

At least four high relief lineaments protrude from the eastern shoreline of the Sua Pan (Figs. 4 and 6). These are collinear to valleys eroded into the higher topography that dominates the eastern edge of the study area. These linear protrusions decease in size from north to south and the smallest is an isolated linear island in the middle of the Sua Pan. The higher topography east of the Sua Pan is offset and terminates abruptly where these valleys merge into the collinear protrusions (Fig. 6c). This gives the impression of right-hand separation along the jetty/spit-valley axes (Fig. 6a and c). These jetty/spit features trend NW-SE and are parallel to each other. Furthermore, on the opposite side of the Sua Pan, just beyond the western shoreline, there are instances of these same linear features that become accentuated in the topographic filter (Fig. 6a). Also in the area is a the 12,384 m^2 Kukome Island comprised of basalts and tapered slightly in the identical NW-SE

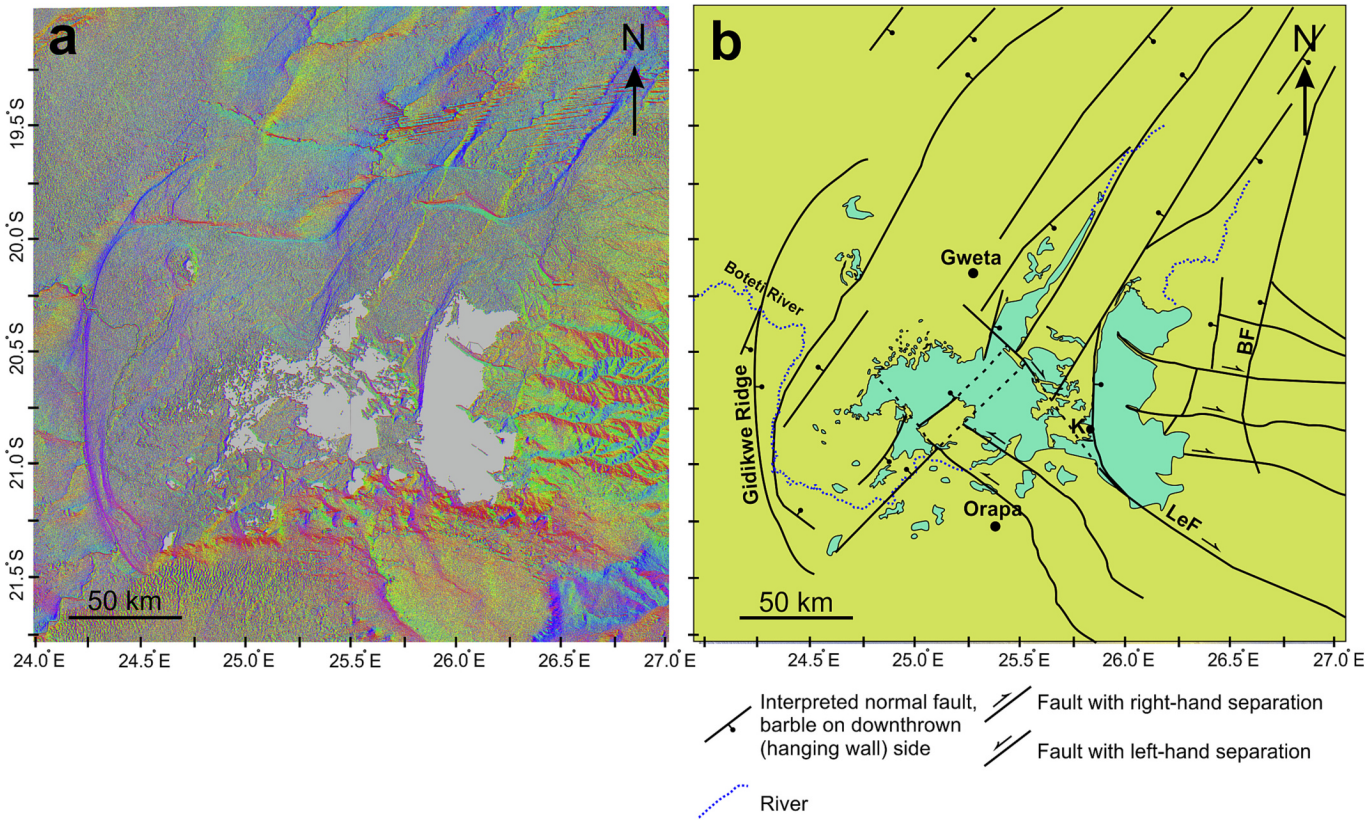

Fig. 4. Fault identification. a) Topographic data run through a Python script following the process of Minin (2016). Red dips northward, yellow dips westward, green dips southward, and blue dips eastward. b) Mapping of the fault scarps observed in Fig. 4a and expanding upon faults mapped in previous studies (Aldiss and Carney, 1992; Barton Jr et al., 1994; Carney et al., 1994; Eckardt et al., 2016; Green et al., 1980; Kooganne et al., 2021; Mapeo et al., 2004). K = Kubu Island. BF = Bushman Fault. LeF = Lechana Fault. Boteti River located on the west side of the basin crossing the Gidikwe Ridge. (For interpretation of the references to color in this figure legend, the reader is referred to the web version of this article.)

direction (Fig. 6).

4.2. Tectonic terrane boundaries

In this section, we describe the older tectonic terranes underlying the Makgadikgadi Basin and determine their position relative to the pans in order to evaluate the extent to which the current Quaternary fault geometry and inferred fault movement is influenced by the fabric of these terranes. With the aid of Bouguer gravity anomaly patterns and existing geologic mapping outside the pans, we have attempted to better constrain the previously proposed terrane boundaries (Fig. 7). We have chosen to place the boundary between the Zimbabwe Craton and the Limpopo-Shashe Belt by extrapolation of that boundary as identified by McCourt et al. (2004). Working on exposed outcrops, these authors defined the boundary as a northwest-trending contact between the Francistown Arc Complex (i.e. the southwestern margin of the Zimbabwe Craton, approximately 2.7 Ga) and the Matsitama-Motloutse Complex (i.e. the Central and Northern Marginal Zones of the Limpopo-Shashe Belt, approximately 2661–2647 Ma). The contact/boundary between the two terrains was defined by the Shashe Shear Zone (McCourt et al., 2004; Ranganai et al., 2002) (Fig. 3). Our extrapolation of the boundary to the northwest intersects the Sua Pan at the northeastern most jetty/spit incursion into Sua Pan (Fig. 6). This location coincides with the northern edge of a high gravity anomaly belt (> -70 mGals) below the eastern Sua Pan shoreline (Fig. 7).

The Limpopo-Shashe Belt boundary can be identified by the low gravity area of the southern side the study area (which coincides with the Mahalapye Granite Complex, Fig. 3a) which transitions northeast to a high gravity anomaly (> -70 mGals) on the eastern side of the study area (coinciding with the Northern Marginal Zone and the Central Zone, Fig. 3). This transition is bounded by the main gravity anomaly at the center of the Sua Pan (black arrows in Fig. 7a). The contact between the Limpopo-Shashe Belt and the Magondi Belt is thus the northeast trending trough (i.e. gravity low) that also coincides with the majority of the western shoreline of the Sua Pan and adjacent to Kubu Island (Fig. 7). This contact also coincides with the dramatic topography change at the southern and eastern margins of the pans (Figs. 2b and 4a). The southern extent of the Ntwetwe Pan and nearby smaller pans also coincides with the southern extent of the Magondi Belt where it terminates against the Limpopo-Shashe Belt.

Several of the normal faults observed in the magnetic data offset the dikes 1.5–2.5 km (Fig. 8a and b). This implies that there is some reactivation of the faults, as well as a small degree of lateral movement. One of these offset locations aligns precisely with the northern section of the Gidikwe Ridge (Fig. 8b and c). An additional eleven faults were inferred from the identification of offset dikes (Fig. 8b and c), bringing the total number of faults presented in this study to 39. These faults were not observed in the DEM filter (Fig. 4a), but share the same general northeast-southwest trend as many of those inferred in Fig. 4b.

The aeromagnetic data can also be used to demonstrate the structural trends in the fabric of the Magondi Belt. A high pass filter removes the low anomaly values and leaves behind only the 100–700 nT range (Fig. 9). Despite interference from the dike swarm, the fabric of the fold belts is apparent, following the NE-SW direction of the faults and sometimes curving to the east. This curvature is particularly evident in the Sua Pan where a high anomaly matches the western shoreline (Fig. 9).

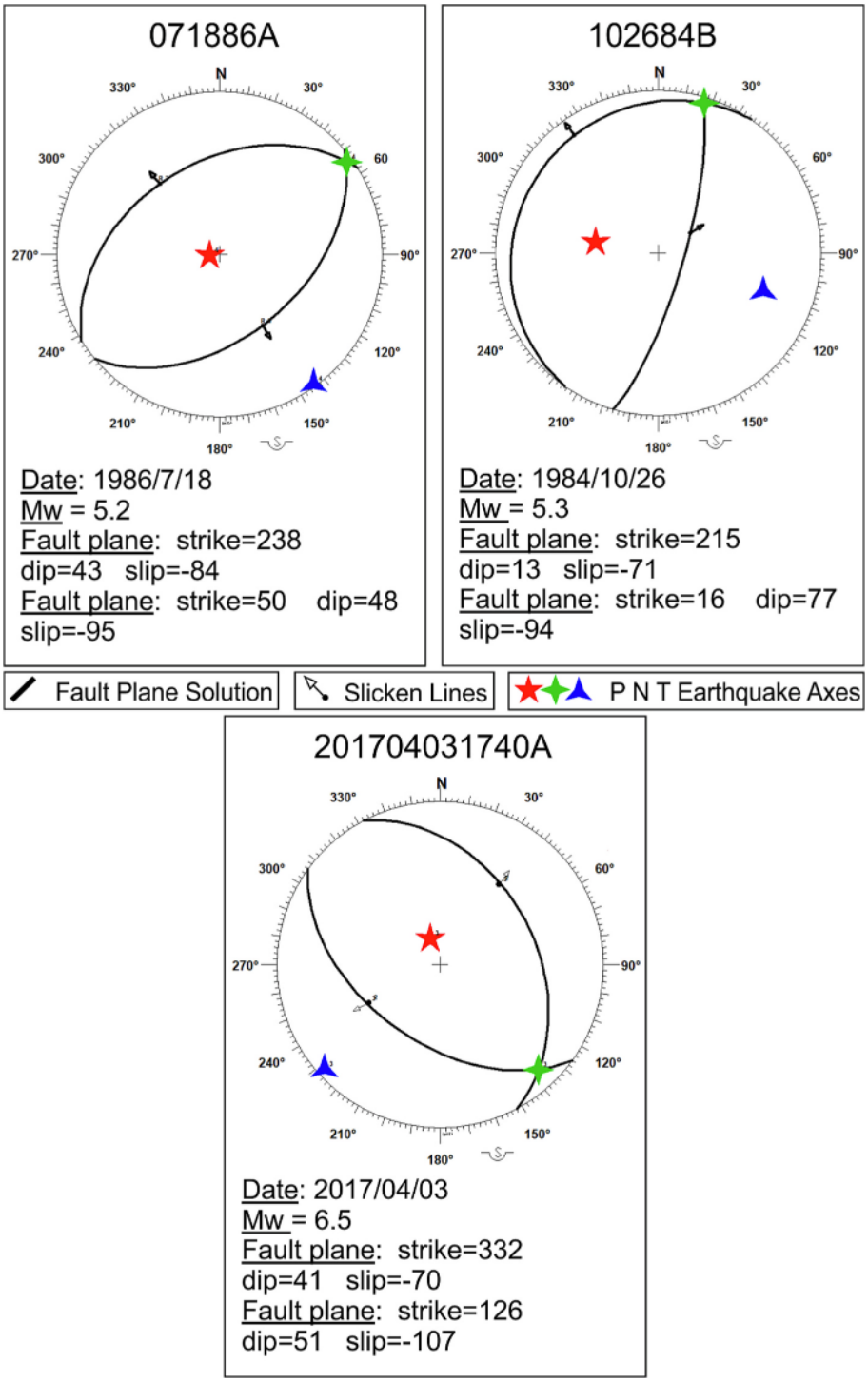

Fig. 5. Moment tensor data of three earthquakes displayed in stereonets. Earthquake epicenters are marked by red points in Fig. 1b. (For interpretation of the references to color in this figure legend, the reader is referred to the web version of this article.)

5. Combined structure

The 28 faults identified from the DEM filter and the 11 faults identified from the total magnetic intensity map (39 in total) are overlain on the proposed tectonic terranes and the outline of the pans to better visualize possible relationships between them (Fig. 10). Fault orientations are measured (Fig. 11). Fault strikes within the entire study area have a dominant 36° trend and three secondary trends of −73°, 2°, and − 44°. Within the Magondi Belt, the Passarge Basin, and the Ghanzi-Chobe Zone there is a dominant 36° trend and a secondary −4° trend. Four of these faults observed curve from a NE-SW (approximately 38°) to a NW-SE (approximately −25°). Within the Limpopo-Shahse Belt there are two closely weighted strikes of −43° and − 67° and a lesser of 13°. There are four northwest-southeast striking right-separation faults perpendicular to the Bushman Fault (Green et al., 1980). Two of these show right separation of a normal fault (Figs. 6 and 10). These faults align with morphological features of the east shoreline of the Sua Pan, where several jetty/spit-like linear features are observed protruding into the pan from the shoreline (Fig. 6).

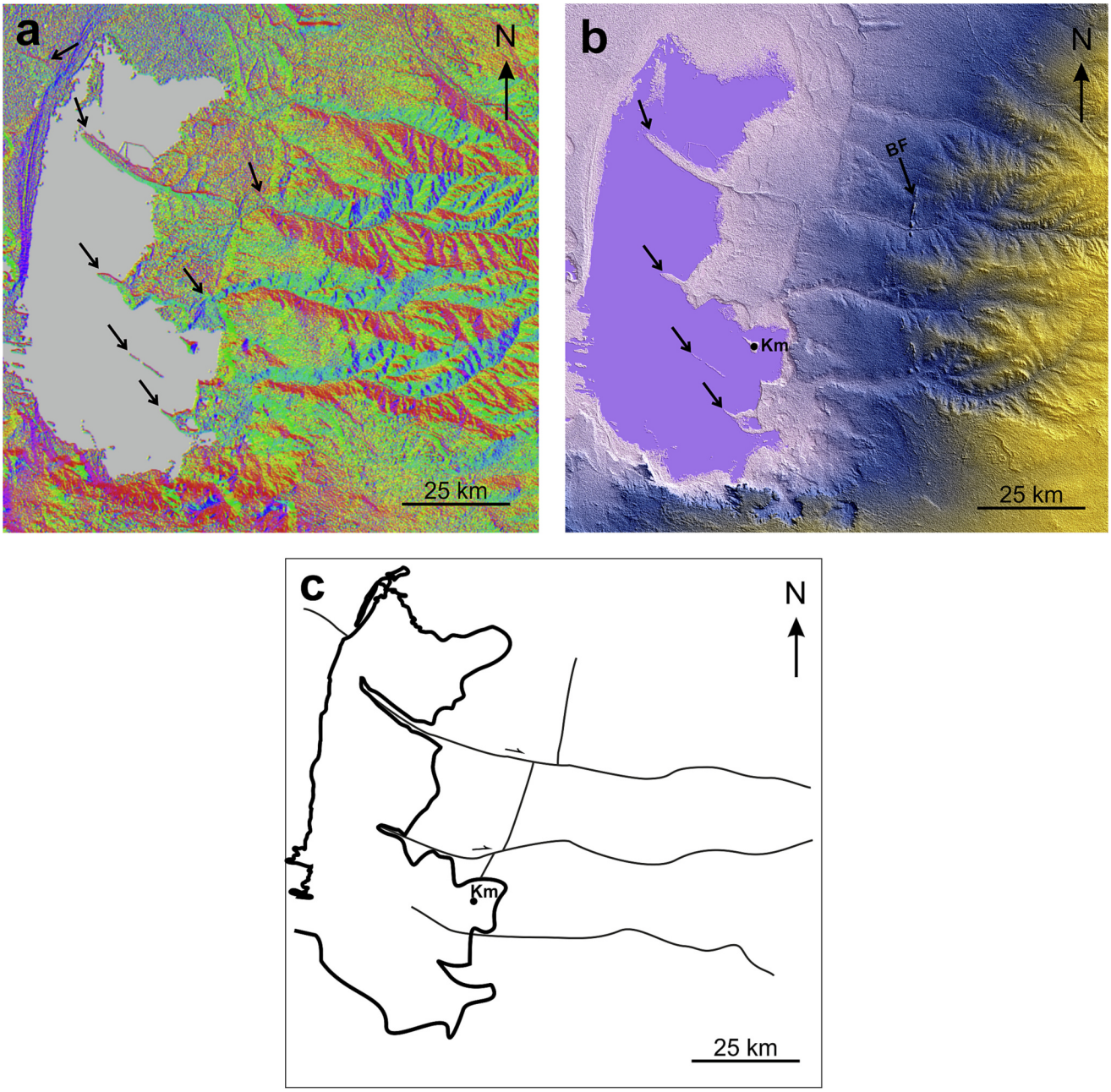

Fig. 6. Close-up of the Sua Pan showing the jetty/spit features that protrude from the eastern shoreline and are collinear to preferentially eroded valleys. a) Close-up of Fig. 4a showing the Sua Pan. Black arrows point to the jetty/spit features, as well as instances where the topography terminates abruptly and appears to be offset. b) Close-up of Fig. 2b showing the Sua Pan. Black arrows point to the jetty/spit features and the Bushman Fault (BF) for reference. c) Outline of the features in a and b. Km = Kukome Island.

6. Discussion and conclusions

We have provided evidence suggesting that the overall geometry of the pans is structurally controlled by both faulting and tectonic terrane boundaries. Although the pans have been suggested to be influenced by earlier tectonic features (Eckardt et al., 2016; Podgorski et al., 2013), the precise relationship had not been fully appreciated. Furthermore, the continuity of faults from the Limpopo Belt (e.g. the Lechana Fault) into the Magondi Belt, as well as how Kubu Island fits into the history of the tectonic terranes (Aldiss and Carney, 1992; Chisenga et al., 2020; Majaule et al., 2001; McCourt et al., 2004) has been a matter of controversy. In general, pan geometry is the result of the intersection of two sets of faults and the contact between the Magondi and Limpopo-Shashe Belts, which themselves have been influenced by the impeding Zimbabwe Craton.

6.1. Fault-pan geometry

Faults tend to have preferred orientations depending on the tectonic terrane they overlie (Figs. 10 and 11). Within the Magondi Belt and Ghanzi-Chobe Zone, the combination of fault scarp dip direction, inference from extension direction derived from earthquake fault plane solutions, and previous proposals by Eckardt et al. (2016) confirm that these faults are mostly normal and create a horst and graben topography. However, offset dikes observed in the aeromagnetic data (Fig. 8) show that fault movement has a strike-slip component as well, and confirms that fault movement at least postdates the Jurassic Okavango Dike Swarm. Aeromagnetic data was very useful in identifying many of

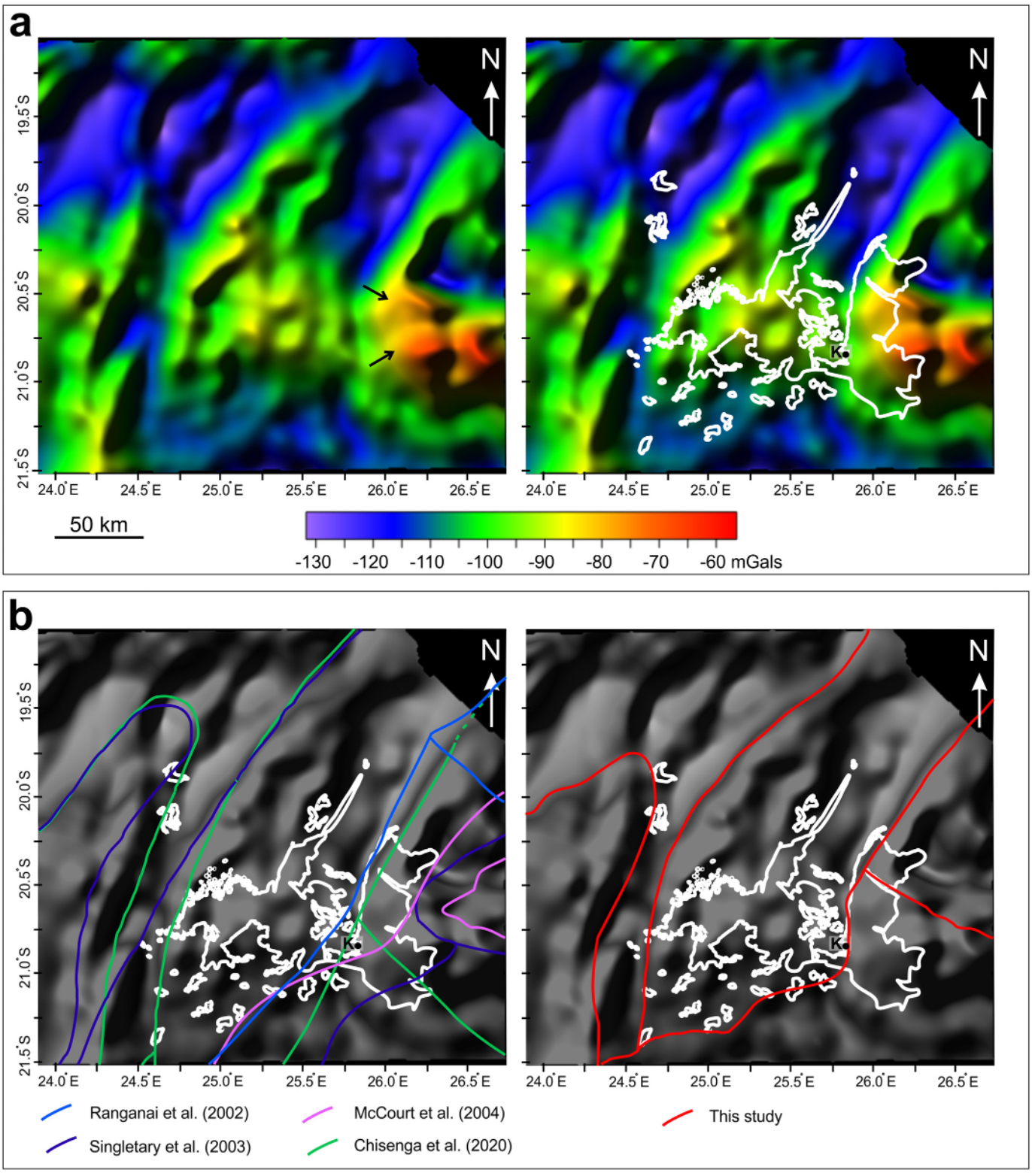

Fig. 7. Bouguer gravity anomaly assisted tectonic terrane boundary investigation. a) Color shaded relief bouguer gravity anomaly map (left) with the outline of the pans in white (right). Black arrows indicate the transition to the high gravity anomaly underneath the Sua Pan b) Grayscale versions of the bouguer gravity anomaly map (for contrast clarity) with the combined previous tectonic terrane boundary interpretations presented in Fig. 3 (left) and the interpretation of this study (right).

the mapped faults, however not all faults have an aeromagnetic signature and were identified from satellite imagery. Faults are identifiable within aeromagnetic data where they cut across and offset layering (e.g. differences in the magnetic susceptibilities of basalt flows that are interlayered with metasediments). Faults that are not identified from aeromagnetic data might be parallel to layering or simply the rocks do not have contrasting magnetic susceptibilities. A dike laterally offset by 150 m below the the Gidikwe Ridge demonstrates that the ridge is fault controlled (Fig. 8b). Since the Gidikwe Ridge has been previously suggested to represent a relic shoreline of Makgadikgadi Paleolake

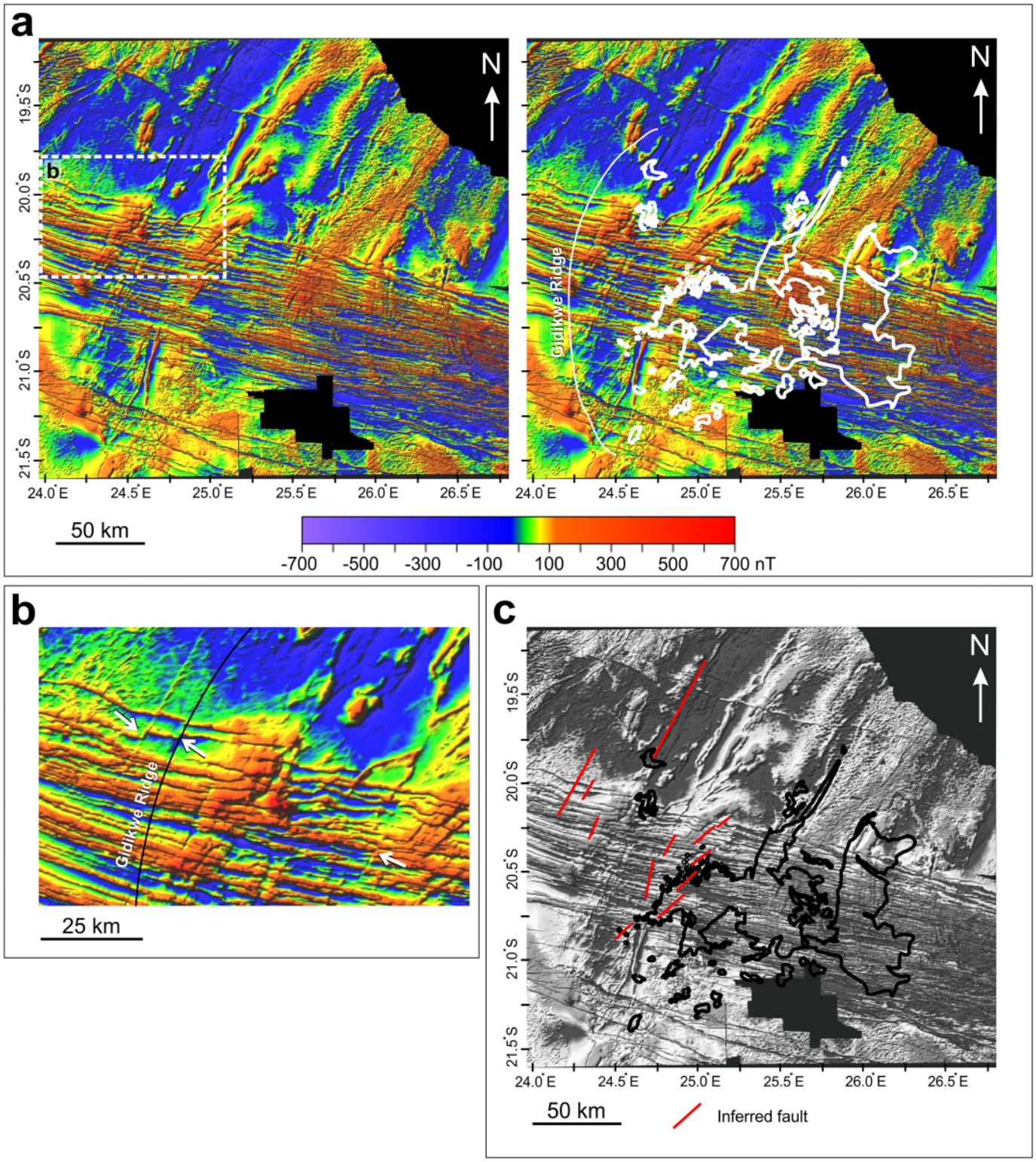

Fig. 8. Total magnetic intensity assisted fault identification. a) Color shaded relief total magnetic intensity map (left) with the outline of the pans and the Gidikwe Ridge in white (right). The west northwest-east southeast trending lineations are the Okavango Dike Swarm (LePera, et al., 2014). Dashed white box marks the location of Fig. 8b. b) Close-up example of offset dikes. White arrows mark specific locations of offset. Black line represents the Gidikwe Ridge which overlies one of the marked offsets. c) Grayscale version of the total magnetic intensity map (for contrast clarity) with inferred faults marked by red lines. (For interpretation of the references to color in this figure legend, the reader is referred to the web version of this article.)

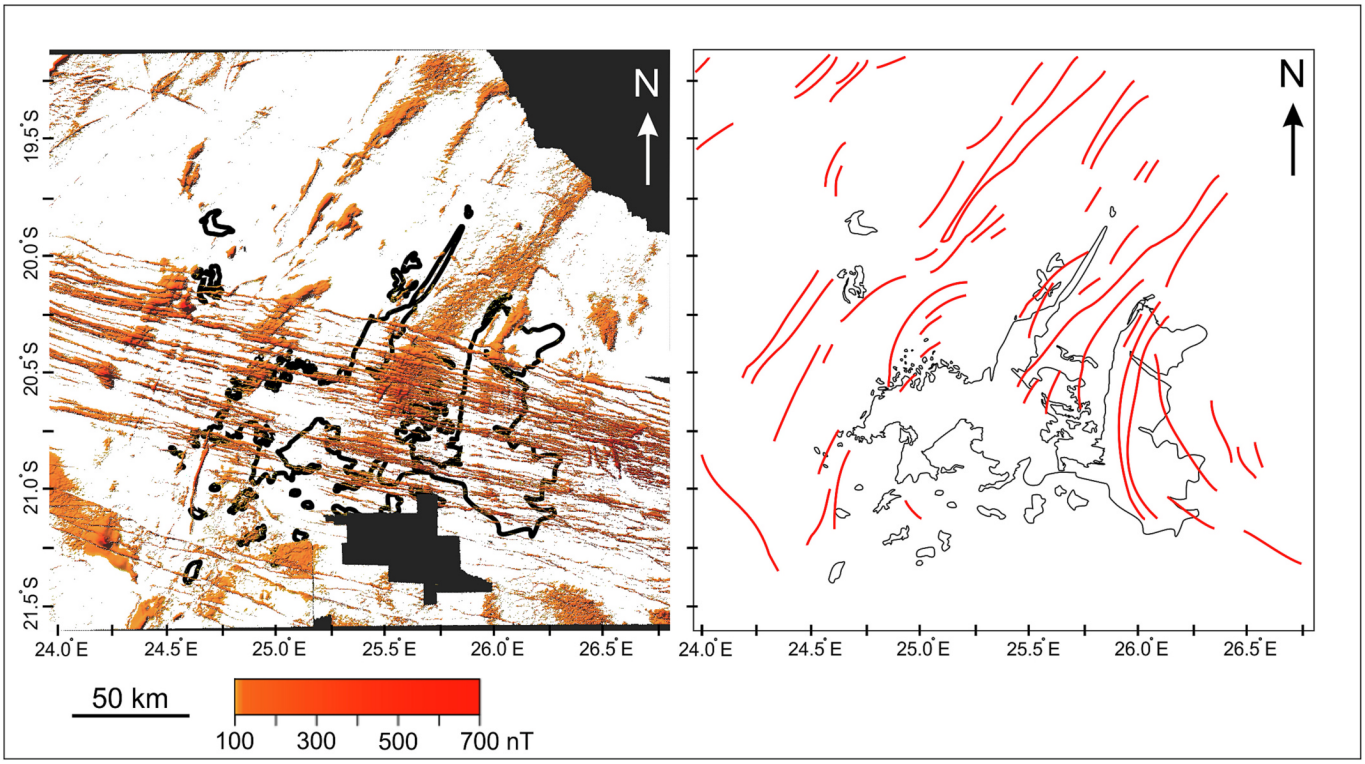

Fig. 9. Filtered magnetic intensity mapping to highlight the 100–700 nT range of high magnetic anomalies (left). The major anomalies are traced in red (right). (For interpretation of the references to color in this figure legend, the reader is referred to the web version of this article.)

(Podgorski et al., 2013; McFarlane and Eckardt, 2006), and the ridge trends in the exact concave shape as the western shoreline of the Sua Pan, it further supports our hypothesis that the shoreline geometry is largely fault controlled. For purposes of this study, we do not discuss the relationship between the faults and the fabric of the fold belts in three dimensional terms (i.e. their intersecting relationships). Although this relationship has been shown to be a valuable aspect of fault vs. tectonic terrane interpretation (e.g. Phillips et al., 2016), the basement depth below the pans is very shallow. Exploration borehole data (De Beers Prospection Botswana Limited, Licences 61, 62, 68, 69, and 75/88) indicates the basement is approximately 200 m below the Karoo sediment infill of the pans. Thus, a discussion of the two-dimensional relationship between the observed structures in the geophysical datasets and the observed surface topography is considered adequate as a first order characterization of the faulting present in the Makgadikgadi Basin.

Some of the faults, or fault segments, coincide precisely with pan shorelines (Fig. 10). The western shoreline of the Sua Pan, for example, is likely the surface expression of an east dipping normal fault which follows the contact between the Limpopo-Shashe Belt and the Magondi Belt. The Magondi Belt is considered to have been thrust over the Limpopo-Shashe Belt, producing a west dipping thrust fault (McCourt et al., 2004; Ranganai et al., 2002). Extensional reactivation of the back-thrust will produce a geometry in which the principal thrust and the newly formed normal fault (i.e. the western shoreline of the Sua Pan) have opposing dips. In this scenario, it is normal that the two faults are separated by some distance, depending on the original length between ramp and flat, as well as the amount of erosion.

Fault controlled shorelines are further attested to by higher silica concentrations on pan margins which is thought to be derived by groundwater (Ringrose et al., 2009). The existence of faults at many of these margins (i.e. shorelines) likely allowed for the movement of groundwater at these margins, and even aided the catchment of water in pools. The high relief lineaments (i.e. jetties/spits) extending from the eastern shoreline of the Sua Pan (Figs. 6 and 10) align with WNW-ESE striking faults and are probably the surface expression of these faults. Their formation and positive relief is possibly due to preferential silcretisation events described previously by Ringrose et al. (2009) where groundwater utilized the preexisting faults (Lekula et al., 2018; McFarlane and Long, 2015). Burrough (2022) interprets these high relief lineaments of the eastern shoreline of the Sua Pan as spits. Spits are depositional features that require prevailing wind and constant current. If these features represent spits, their decrease in size from north to south (Fig. 6) might imply that depositional energy decreased southward, the lake level was maintained for a longer duration in the north, or the river was entering the Sua Pan in different locations overtime in a specific north-south trend. Rivers may have entered the pan along the fault pathways (preferentially eroding the observed valleys east of the Sua Pan) and aided in spit formation. However, due to the fact that Kukome Island (Fig. 6) is made of basalt, the relationship between these high relief lineaments, faulting, sedimentation, and the Okavango Dike Swarm may not have a simple explanation. We argue it is unlikely several parallel lineaments, collinear with faults, are solely the products of sedimentation dependent on prevailing wind directions and likely have a relationship with the inferred faults.

The western shoreline of the Ntwetwe Pan, although less defined than the western shoreline of the Sua Pan, has several coinciding northeast-southwest striking faults. Layered mounds identified by Franchi et al. (2020) on the western side of the Ntwetwe Pan might also reflect erosional differences that are in part contributed to by these faults. The river entering the western side of the Ntwetwe is deflected and rerouted twice by faults. It enters the study area, possibly following a northwest-southeast striking fault extending from the Limpopo Belt and is deflected southward by a fault that runs parallel with the Gidikwe Ridge. It then returns to a southeast direction coinciding with another northwest-southeast striking fault extending from the Limpopo-Shashe Belt (Fig. 10).

In as much as the WNW-ESE-striking faults within the Limpopo-Shashe Belt just south of the Zimbabwe Craton (Fig. 10) overlie and

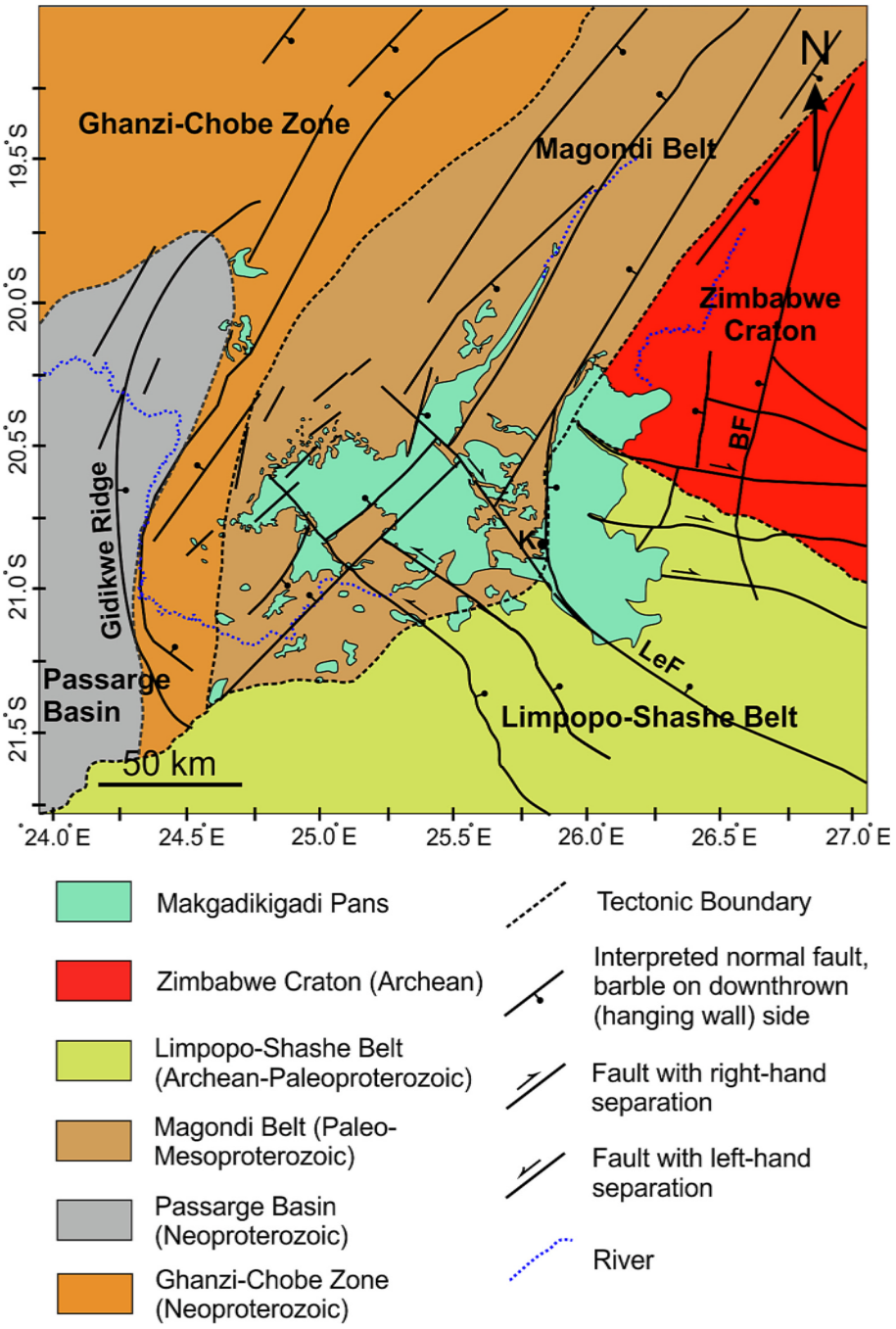

Fig. 10. Faults from Fig. 3b superimposed over our proposed tectonic terrane boundaries. K = Kubu Island. BF = Bushman Fault. LeF = Lechana Fault.

have the same trend as the magnetic anomalies produced by the Okavango Dike Swarm, they may have been controlled by the dikes. These faults cut into the eastern Sua Pan and right separate a northeast-striking normal fault. Because they do not appear to offset the Bushman Fault, latest movement on the Bushman Fault is also probably Quaternary.

The fault propogating from the Limpopo-Shashe Belt, passing just south of Kubu Island, and crossing the entire Ntwetwe Pan is likely the Lechana Fault (Aldiss, 1991; Aldiss and Carney, 1992; Carney et al., 1994; McCourt et al., 2004), or possibly a fault related to the Sunny Side Shear Zone (Ranganai et al., 2002) (Fig. 10). Other faults parallel to the Lechana Fault and extending from the southeast (Fig. 10) thus represent faults within the Northern and Central Marginal Zones of the Limpopo-Shashe Belt bounded by the Shashe Shear Zone and the Sunny Side Shear Zone. These faults extending from the Limpopo Belt are identified to pass into the Magondi Belt where they intersect with the northeast-southwest striking rift related faults. High relief lineaments on the northeast margin of the Ntwetwe Pan (Fig. 2a) are likely the surface expression of the Lechana Fault and, like the jetties/spits in the Sua Pan, are proposed to share a similar silcretisation formation process described by Ringrose et al. (2009). As described earlier the Lechana Fault at this location right separates the northeast-striking normal fault that controls the northeastern boundary of Ntwetwe Pan. At least one other northwest-striking fault left separates a northeast-striking normal fault on the southeast boundary of the pan.

In the case of the concave-eastward curved rift belt structures of the pans, the curvature of those faults overlying the Ghanzi-Chobe Zone and Magondi Belt, like the Gidikwe Ridge Fault, is controlled, or at least influenced by, the curvature of the belts themselves (Figs. 8 and 9). The

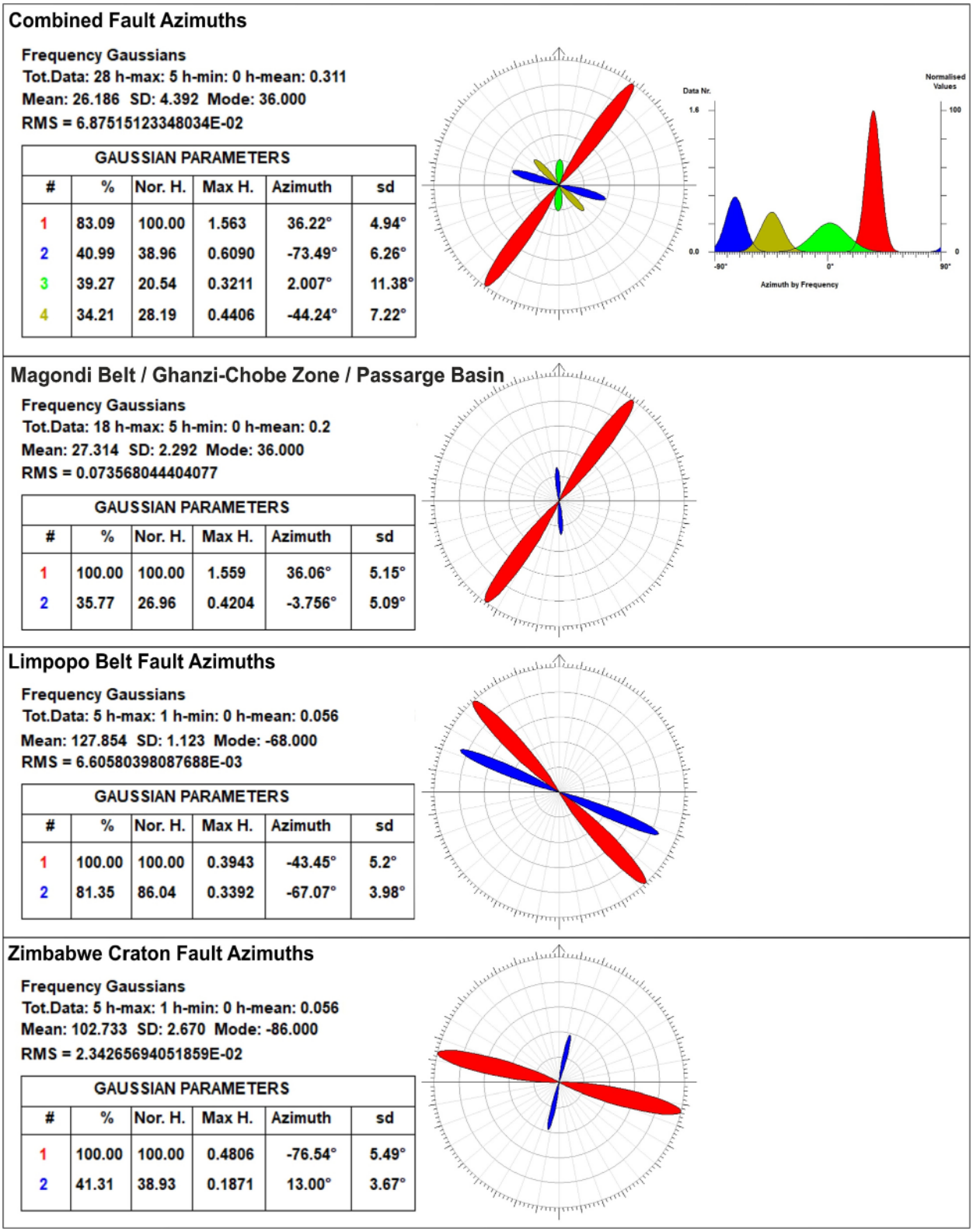

Fig. 11. Rose diagrams showing the combined azimuths of the faults presented in Fig. 4b. Fault azimuths were found to have four distinct groupings. The four groups are color coded and listed 1–4 in the table in order of frequency magnitude, red being the group with the highest frequency and brown being the group with the lowest frequency. (For interpretation of the references to color in this figure legend, the reader is referred to the web version of this article.)

curvature of the faults overlying the Limpopo-Shashe Belt, like the southern part of the Lechana Fault and the two other faults to the east of it (Fig. 10), has been accentuated by the influence of the adjacent northwest trending Limpopo-Shashe Belt. Although the actual movement direction of these faults is unknown, we infer from the DEM morphology that they dip to the northeast. If the NE-SW extension direction determined from fault plane solutions for the 2017 earthquake, 80 km south of the study area can be applied to these faults, they are

down-to-the northeast normal faults as shown on Figs. 4b and 10. The same change in extension direction was observed previously by Delvaux and Barth (2010) between the Luangwa Graben (Fig. 1) and South Africa and it is likely that the Makgadikgadi Basin represents the point where this change occurs. Admittedly, the distance between the available focal mechanisms (071886A and 102684B at Lake Kariba and 201704031740A just south of the study area) is approximately 700 km (Fig. 1). Although one sees strain rotations across distances of <100 km in East Africa (Morely, 2010; Rajabi et al., 2022; Williams et al., 2019), the available data nevertheless suggests that in the bigger picture, significant strain rotation (i.e. nearly 180° rotation) within the San Plate exists. This observation might be important in constraining the relationship between the Nubian and San Plates (Wedmore et al., 2021) and more broadly the rigidity of the San Plate in future work.

6.2. Updated tectonic terrane boundaries

Our updated tectonic terrane boundaries more accurately represent observations of gravity and magnetic structures, and fault orientations. Our interpretation of the Magondi and Limpopo-Shashe Belt contact south of the pans is more agreeable with McCourt et al. (2004) than Ranganai et al. (2002), Chisegna et al. (2020), and Singletary et al. (2003), whereas our Passarge Basin boundary is mostly agreeable with Chisegna et al. (2020). However, we suggest that the northernmost extent of the Passarge Basin terminates about 50 km further south than the boundary proposed by both Chisenga et al. (2020) and Singletary (2002), based on the structures observed in the aeromagnetic and gravity data (Figs. 7, 8, and 9). The Nxai and Kudiakam Pans (Figs. 2a and 10) mark the eastern boundary of the Passarge Basin, along with the Gidikwe Ridge.

The boundary between the Zimbabwe Craton and the Limpopo-Shashe Belt is elusive and difficult to constrain (Barton et al., 1994; Aldiss, 1991; McCourt et al., 2004; Ranganai et al., 2002). Previous studies have placed this boundary within the study area (Fig. 3), but in differing locations either east (McCourt et al., 2004; Singletary et al., 2003), northeast (Ranganai et al., 2002), or below the Sua Pan. Barton et al. (1994) determined from insitu analyses of deposits associated with the Bushman Fault (just west of the Sua Pan approximately 20.5° S, 26.5° E) that the rocks in which the Bushman Fault occurs is generally distinct from the Zimbabwe Craton. This supports the interpretation of gravity data from Ranganai et al. (2002), which placed the boundary further east. If the boundary between the Zimbabwe Craton and the Limpopo-Shashe Belt is brought south to the location proposed by Chisenga et al. (2020), the marginal zones (i.e. Central and Northern Marginal Zones) indicated by McCourt et al. (2004) and Ranganai et al. (2002) are pinched out by the time they reach the Magondi Belt. This would contradict field observations and mapping in the area (McCourt et al., 2004). We have drawn the boundary (Figs. 7c and 10) from where it was mapped by McCourt et al. (2004) into the northernmost part of Sua Pan. For these reasons we suggest that, although the Zimbabwe Craton did not directly control fault trends in the pans, it nevertheless had a major structural influence on the pans by controlling both the structure of the Central and Northern Marginal Zones, and the southern Magondi Belt.

6.3. Summary and conclusions

In summary, the northeast-striking, rift-related normal faults in the northern part of the pans follow the trend of the folds (magnetic anomalies) within the underlying Magondi Belt in a similar way that normal faults in the Okavango Rift Zone in northwestern Botswana follow the trend of structures in the Neoproterozoic Ghanzi-Chobe Zone (Kinabo et al., 2007, 2008; Modidi et al., 2000; Chisenga et al., 2020). In the western and central part of the pans the pronounced change in strike of the faults to a concave-eastward curvature follows the curved trace of the structures in the southern Magondi Belt that were produced by the impingement of the developing fold belt against the Zimbabwe Craton. This is similar to the concave-eastward curve of the Tanganyika Rift Belt to the north that follows the underlying Paleoproterozoic Ubendiam Belt that wrapped around the Tanzania Craton (e.g., Hanson, 2003; McCourt et al., 2014).

The structural components underlying the Makgadikgadi Pans describe a complex tectonic regime. Shorelines mimicking regional structures in magnetic and gravity data, in combination with fault strikes and movement, show that they are indeed structurally controlled. The existence of high relief structures on the pan floor which coincide with identified faults may represent groundwater processes which utilize faults and may be a lucrative area of future work in constraining the regional groundwater activity in northwestern Botswana. Furthermore, the relationship between the Bushman Shear Zone (Barton et al., 1994) and the Shashe Shear Zone (Ranganai et al., 2002) is likely an important factor in the evolution of the eastern shoreline of the Sua Pan, but still remains to be fully understood. In short, despite the pans representing the southernmost extent of the EAR in which the faults already have formed collinear to the other rift sections further to the northeast, the preexisting fabric of the tectonic terranes also has a direct influence on fault propagation and in turn modulates the geometry of the pans. Future work might include seismic or electrical resistivity surveying along the shorelines and the Gidikwe Ridge to further investigate the subsurface nature of these faults.

CRediT authorship contribution statement

G. Schmidt: Conceptualization, Methodology, Formal analysis, Investigation, Resources, Data curation, Writing – original draft, Writing – review & editing, Visualization, Project administration, Funding acquisition. **F. Franchi:** Formal analysis, Investigation, Resources, Data curation, Writing – original draft, Writing – review & editing, Visualization, Project administration, Funding acquisition. **F. Salvini:** Conceptualization, Methodology, Writing – original draft, Writing – review & editing, Supervision, Funding acquisition. **A.T. Selepeng:** Methodology, Formal analysis, Resources, Data curation, Writing – original draft. **E. Luzzi:** Writing – original draft, Writing – review & editing. **C. Schmidt:** Conceptualization, Methodology, Writing – original draft, Writing – review & editing. **E.A. Atekwana:** Resources, Data curation, Writing – original draft, Writing – review & editing.

Declaration of Competing Interest

The authors declare the following financial interests/personal relationships which may be considered as potential competing interests:

Gene Schmidt reports financial support was provided by Europlanet Society. A co-author of the manuscript, Dr. Francesco Salvini, is also an editor for the Tectonophysics journal.

Data availability

Data will be made available on request.

Acknowledgments

We would like to thank Kabelo Hlabano (BIUST) for his assistance in the field. The field work was funded by Europlanet 2024 RI transnational access awarded to Gene Schmidt and Erica Luzzi (application n. 20-EPN2-121). Europlanet 2024 RI has received funding from the European Union's Horizon 2020 research and Innovation Programme under grant agreement no. 871149. Further field activities and analyses carried out under the research permit number MOTE/1/18/6 x (23) attributed to Fulvio Franchi. Laboratory work and data analyses were funded by GeoQuTe Lab (Laboratorio di Geodinamica Quantitativa e Telerilevamento) of Roma Tre University.

References

Aldiss, D.T., 1991. The Motloutse complex and the Zimbabwe craton/Limpopo belt transition in Botswana. Precambrian Res. 50 (1–2), 89–109. https://doi.org/10.1016/0301-9268(91)90049-G.

Aldiss, D.T., Carney, J.N., 1992. The geology and regional correlation of the Proterozoic Okwa Inlier, western Botswana. Precambrian Res. 56 (3–4), 255–274. https://doi.org/10.1016/0301-9268(92)90104-V.

Baillieul, T.A., 1979. Makgadikgadi pans complex of Central Botswana. Geol. Soc. Am. Bull. 90 (2_Part_II), 289–312. https://doi.org/10.1130/GSAB-P2-90-289.

Barton Jr., J.M., Blaine, J.L., Doig, R., Byron, C.L., 1994. The geological setting and style of copper mineralization at the Bushman group of deposits, northeastern Botswana. J. Afr. Earth Sci. 18 (2), 87–97. https://doi.org/10.1016/0899-5362(94)90022-1.

Begg, G.C., Griffin, W.L., Natapov, L.M., O'Reilly, S.Y., Grand, S.P., O'Neill, C.J., Bowden, P., 2009. The lithospheric architecture of Africa: seismic tomography, mantle petrology, and tectonic evolution. Geosphere 5 (1), 23–50. https://doi.org/10.1130/GES00179.1.

Blue Marble Geographics, 2011. Global Mapper [Computer Software].

Bufford, K.M., Atekwana, E.A., Abdelsalam, M.G., Shemang, E., Atekwana, E.A., Mickus, K., Molwalefhe, L., 2012. Geometry and faults tectonic activity of the Okavango Rift Zone, Botswana: evidence from magnetotelluric and electrical resistivity tomography imaging. J. Afr. Earth Sci. 65, 61–71.

Burrough, S.L., 2022. The Makgadikgadi Basin. In: Landscapes and Landforms of Botswana. Springer, Cham, pp. 77–90.

Burrough, S.L., Thomas, D.S., Bailey, R.M., 2009. Mega-Lake in the Kalahari: a Late Pleistocene record of the Palaeolake Makgadikgadi system. Quat. Sci. Rev. 28 (15–16), 1392–1411.

Carney, J.N., Aldiss, D.T., Lock, N.P., 1994. The Geology of Botswana. Botswana Geol. Surv. Bull. 37, 113p.

Chisenga, C., Jianguo, Y., Fadel, I., van der Meijde, M., Atekwana, E.A., 2020. Updated tectonic terrane boundaries of Botswana determined from gravity and aeromagnetic data. Episodes J. Int. Geosci. 43 (4), 919–933. https://doi.org/10.18814/epiiugs/2020/020054.

Cooke, H.J., 1980. Landform evolution in the context of climatic change and neo-tectonism in the Middle Kalahari of north-central Botswana. Trans. Inst. Br. Geogr. 80–99.

Crameri, F., Shephard, G.E., Heron, P.J., 2020. The misuse of colour in science communication. Nat. Commun. 11 (1), 1–10.

Daly, M.C., Green, P., Watts, A.B., Davies, O., Chibesakunda, F., Walker, R., 2020. Tectonics and landscape of the Central African Plateau and their implications for a propagating Southwestern Rift in Africa. Geochem. Geophys. Geosyst. 21 (6) e2019GC008746.

Delvaux, D., Barth, A., 2010. African stress pattern from formal inversion of focal mechanism data. Tectonophysics 482 (1–4), 105–128. https://doi.org/10.1016/j.tecto.2009.05.009.

Dziewonski, A.M., Chou, T.-A., Woodhouse, J.H., 1981. Determination of earthquake source parameters from waveform data for studies of global and regional seismicity. J. Geophys. Res. 86, 2825–2852. https://doi.org/10.1029/JB086iB04p02825.

Eckardt, F.D., Cotterill, F.P., Flügel, T.J., Kahle, B., McFarlane, M., Rowe, C., 2016. Mapping the surface geomorphology of the Makgadikgadi Rift Zone (MRZ). Quat. Int. 404, 115–120.

Ekström, G., Nettles, M., Dziewonski, A.M., 2012. The global CMT project 2004-2010: Centroid-moment tensors for 13,017 earthquakes. Phys. Earth Planet. Inter. 200-201, 1–9. https://doi.org/10.1016/j.pepi.2012.04.002.

Evans, R.L., Elsenbeck, J., Zhu, J., Abdelsalam, M.G., Sarafian, E., Mutamina, D., Jones, A.G., 2019. Structure of the lithosphere beneath the Barotse Basin, western Zambia, from magnetotelluric data. Tectonics 38 (2), 666–686. https://doi.org/10.1029/2018TC005246.

Fadel, I., van der Meijde, M., Paulssen, H., 2018. Crustal structure and dynamics of Botswana. J. Geophys. Res. Solid Earth 123 (12), 10–659. https://doi.org/10.1029/2018JB016190.

Franchi, F., MacKay, R., Selepeng, A.T., Barbieri, R., 2020. Layered mound, inverted channels and polygonal fractures from the Makgadikgadi pan (Botswana): possible analogues for Martian aqueous morphologies. Planet. Space Sci. 192, 105048 https://doi.org/10.1016/j.pss.2020.105048.

Franchi, F., Cavalazzi, B., Evans, M., Filippidou, S., Mackay, R., Malaspina, P., Nisejuenabgm, G., Price, A., Rossi, V., 2022. Late Pleistocene–Holocene palaeoenvironmental evolution of the Makgadikgadi Basin, Central Kalahari, Botswana: new evidence from shallow sediments and ostracod fauna. Front. Ecol. Evol. 10, 818417.

Green, D., Crockett, R.N., Jones, M.T., 1980. Tectonic control of Karoo sedimentation in mid-eastern Botswana. S. Afr. J. Geol. 83 (2), 213–219.

Grey, D.R.C., Cooke, H.J., 1977. Some problems in the Quaternary evolution of the landforms of northern Botswana. Catena 4 (1–2), 123–133. https://doi.org/10.1016/0341-8162(77)90014-5.

Grove, A.T., 1969. Landforms and climatic change in the Kalahari and Ngamiland. Geogr. J. 135 (2), 191–212.

Hanson, R.E., 2003. Proterozoic geochronology and tectonic evolution of southern Africa. Geol. Soc. Lond., Spec. Publ. 206 (1), 427–463.

Hlatywayo, D.J., 1995. Fault-plane solutions of the Deka Fault zone and mid-Zambezi Valley. Geophys. J. Int. 120 (3), 567–576.

Kebede, F., Kulhánek, O., 1991. Recent seismicity of the East African Rift system and its implications. Phys. Earth Planet. Inter. 68 (3–4), 259–273. https://doi.org/10.1016/0031-9201(91)90045-J.

Key, R.M., Ayres, N., 2000. The 1998 edition of the national geological map of Botswana. J. Afr. Earth Sci. 30 (3), 427–451.

Kinabo, B.D., Atekwana, E.A., Hogan, J.P., Modisi, M.P., Wheaton, D.D., Kampunzu, A. B., 2007. Early structural development of the Okavango rift zone, NW Botswana. J. Afr. Earth Sci. 48 (2–3), 125–136. https://doi.org/10.1016/j.jafrearsci.2007.02.005.

Kinabo, B.D., Hogan, J.P., Atekwana, E.A., Abdelsalam, M.G., Modisi, M.P., 2008. Fault growth and propagation during incipient continental rifting: Insights from a combined aeromagnetic and shuttle Radar Topography Mission digital elevation model investigation of the Okavango Rift Zone, Northwest Botswana. Tectonics 27 (3). https://doi.org/10.1029/2007TC002154.

Kolawole, F., Atekwana, E.A., Malloy, S., Stamps, D.S., Grandin, R., Abdelsalam, M.G., Shemang, E.M., 2017. Aeromagnetic, gravity, and differential interferometric synthetic aperture radar analyses reveal the causative fault of the 3 April 2017 Mw 6.5 Moiyabana, Botswana, earthquake. Geophys. Res. Lett. 44 (17), 8837–8846.

Kooganne, A., Imai, A., Agangi, A., Takahashi, R., 2021. Geology, mineralogy, and sulfur isotopes of the Mowana copper deposit, Matsitama Schist Belt, NE Botswana. Resour. Geol. 71 (4), 320–338. https://doi.org/10.1111/rge.12263.

Le Pera, A.K., 2014. Structure and emplacement of the giant Okavango Dike Swarm in Northern Botswana: a new perspective from airborne geophysical data. Oklahoma State University.

Lekula, M., Lubczynski, M.W., Shemang, E.M., 2018. Hydrogeological conceptual model of large and complex sedimentary aquifer systems–Central Kalahari Basin. Phys. Chem. Earth Parts A/B/C 106, 47–62. https://doi.org/10.1016/j.pce.2018.05.006.

Majaule, T., Hanson, R.E., Key, R.M., Singletary, S.J., Martin, M.W., Bowring, S.A., 2001. The Magondi Belt in Northeast Botswana: regional relations and new geochronological data from the Sua Pan area. J. Afr. Earth Sci. 32 (2), 257–267. https://doi.org/10.1016/S0899-5362(01)90006-5.

Mapeo, R.B.M., Ramokate, L.V., Armstrong, R.A., Kampunzu, A.B., 2004. U-Pb zircon age of the upper Palapye group (Botswana) and regional implications. J. Afr. Earth Sci. 40 (1–2), 1–16. https://doi.org/10.1016/j.jafrearsci.2004.08.001.

McCourt, S., Kampunzu, A.B., Bagai, Z., Armstrong, R.A., 2004. The crustal architecture of Archaean terranes in Northeastern Botswana. S. Afr. J. Geol. 107 (1–2), 147–158. https://doi.org/10.2113/107.1-2.147.

McFarlane, M.J., Eckardt, F.D., 2006. Lake Deception: a new Makgadikgadi palaeolake. Botswana Notes Rec. 38, 195–201.

McFarlane, M.J., Long, C.W., 2015. Pan floor 'barchan'mounds, Ntwetwe Pan, Makgadikgadi, Botswana: Their origin and palaeoclimatic implications. Quat. Int. 372, 108–119. https://doi.org/10.1016/j.quaint.2014.10.008.

Miensopust, M.P., Jones, A.G., Muller, M.R., Garcia, X., Evans, R.L., 2011. Lithospheric structures and Precambrian terrane boundaries in northeastern Botswana revealed through magnetotelluric profiling as part of the Southern African Magnetotelluric Experiment. J. Geophys. Res. Solid Earth 116 (B2). https://doi.org/10.1029/2010JB007740.

Minin, M., 2016. In: Minin, M. (Ed.), Quantification and Extraction of Surface Features from Digital Terrain Models. Brock University M.Sc.Earth Sciences Collections.

Modie, B.N., 2000. Geology and mineralisation in the Meso-to Neoproterozoic Ghanzi-Chobe Belt of Northwest Botswana. J. Afr. Earth Sci. 30 (3), 467–474. https://doi.org/10.1016/S0899-5362(00)00032-4.

Modisi, M.P., Atekwana, E.A., Kapunzu, A.B., Mgwisanyi, T.H., 2000. Rift kinematics during the incipient stages of continental fragmentation: evidence from the nascent Okavango Rift, Northwest Botswana. Geology 28, 939–942.

Moore, A.E., Cotterill, F.P.D., Eckardt, F.D., 2012. The evolution and ages of Makgadikgadi palaeo-lakes: consilient evidence from Kalahari drainage evolution south-Central Africa. S. Afr. J. Geol. 115 (3), 385–413. https://doi.org/10.2113/gssajg.115.3.385.

Phillips, T.B., Jackson, C.A., Bell, R.E., Duffy, O.B., Fossen, H., 2016. Reactivation of intrabasement structures during rifting: A case study from offshore southern Norway. J. Struct. Geol. 91, 54–73.

Podgorski, J.E., Green, A.G., Kgotlhang, L., Kinzelbach, W.K., Kalscheuer, T., Auken, E., Ngwisanyi, T., 2013. Paleo-megalake and paleo-megafan in southern Africa. Geology 41 (11), 1155–1158. https://doi.org/10.1130/G34735.1.

Rajabi, M., Esterle, J., Heidbach, O., Travassos, D., Fumo, S., 2022. Characterising the contemporary stress orientations near an active continental rifting zone: a case study from the Moatize Basin, Central Mozambique. Basin Res. https://doi.org/10.1111/bre.12660.

Ranganai, R.T., Kampunzu, A.B., Atekwana, E.A., Paya, B.K., King, J.G., Koosimile, D.I., Stettler, E.H., 2002. Gravity evidence for a larger Limpopo Belt in southern Africa and geodynamic implications. Geophys. J. Int. 149 (3), F9–F14. https://doi.org/10.1046/j.1365-246X.2002.01703.x.

Riedel, F., Henderson, A.C.G., Heußner, K.U., Kaufmann, G., Kossler, A., Leipe, C., Shemang, E., Taft, L., 2014. Dynamics of a Kalahari long-lived mega-lake system—hydromorphological and limnological changes in the Makgadikgadi Basin (Botswana) during the terminal 50 ka. Hydrobiologia 739, 25–53. https://doi.org/10.1007/s10750-013-1647-x.

Ringrose, S., Harris, C., Huntsman-Mapila, P., Vink, B.W., Diskins, S., Vanderpost, C., Matheson, W., 2009. Origins of strandline duricrusts around the Makgadikgadi Pans (Botswana Kalahari) as deduced from their chemical and isotope composition. Sediment. Geol. 219 (1–4), 262–279.

Salvini, F., Billi, A., Wise, D.U., 1999. Strike-slip fault-propagation cleavage in carbonate rocks: the Mattinata Fault Zone, Southern Apennines, Italy. J. Struct. Geol. 21 (12), 1731–1749. https://doi.org/10.1016/S0191-8141(99)00120-0.

Schaller, M., Steiner, O., Studer, I., Holzer, L., Herwegh, M., Kramers, J.D., 1999. Exhumation of Limpopo Central Zone granulites and dextral continent-scale transcurrent movement at 2.0 Ga along the Palala shear zone, Northern Province, South Africa. Precambrian Res. 96 (3–4), 263–288. https://doi.org/10.1016/S0301-9268(99)00015-7.

Schmidt, M., Fuchs, M., Henderson, A.C.G., Kossler, A., Leng, M.J., Mackay, A.W., Shemang, E., Riedel, F., 2017. Paleolimnological features of a mega-lake phase in the Makgadikgadi Basin (Kalahari, Botswana) during Marine Isotope Stage 5 inferred from diatoms. J. Paleolimnol. 58, 373–390. https://doi.org/10.1007/s10933-017-9984-9.

Singletary, S.J., Hanson, R.E., Martin, M.W., Crowley, J.L., Bowring, S.A., Key, R.M., Krol, M.A., 2003. Geochronology of basement rocks in the Kalahari Desert, Botswana, and implications for regional Proterozoic tectonics. Precambrian Res. 121 (1–2), 47–71. https://doi.org/10.1016/S0301-9268(02)00201-2.

Thomas, D., Shaw, P.A., 1991. The Kalahari Environment. Cambridge University Press.

Wedmore, L.N., Biggs, J., Floyd, M., Fagereng, Å., Mdala, H., Chindandali, P., Mphepo, F., 2021. Geodetic constraints on cratonic microplates and broad strain during rifting of thick Southern African lithosphere. Geophys. Res. Lett. 48 (17) https://doi.org/10.1029/2021GL093785 e2021GL093785.

Williams, J.N., Fagereng, Å., Wedmore, L.N., Biggs, J., Mphepo, F., Dulanya, Z., Blenkinsop, T., 2019. How do variably striking faults reactivate during rifting? Insights from southern Malawi. Geochem. Geophys. Geosyst. 20 (7), 3588–3607. https://doi.org/10.1029/2019GC008219.